Materials Science-Poland, 38(4), 2020, pp. 601-612
http://www.materialsscience.pwr.wroc.pl/
DOI: 10.2478/msp-2020-0065

sciendo

Facile preparation of $Co@Co_3O_4$@Nitrogen doped carbon composite from ionic liquid as anode material for high performance lithium-ion batteries

MINGJUN XIAO[1], YANSHUANG MENG[1,3,*], CHAOYU DUAN[1], FULIANG ZHU[1,3], YUE ZHANG[2]

[1]School of Materials Science and Engineering, Lanzhou University of Technology, Lanzhou 730050, China
[2]Department of Manufacturing Engineering, Georgia Southern University, Statesboro, Georgia 30458, United States
[3]State Key Laboratory of Advanced Processing and Recycling of Non-ferrous Metals, Lanzhou 730050, China

$Co@Co_3O_4$@Nitrogen doped carbon ($Co@Co_3O_4$@NDC) composite is synthesized by high temperature carbonization of ionic liquids followed by low temperature thermal oxidation. In the process of high temperature carbonization, cobalt ions are reduced to metallic cobalt, producing Co@Nitrogen doped carbon (Co@NDC). $Co@Co_3O_4$@NDC composite is obtained after low temperature oxidation, in which a part of the metallic cobalt is oxidized to Co_3O_4. The structural characterizations indicate that the composite is composed of three crystalline phases (carbon, Co and Co_3O_4). The results of transmission electron microscopy study show that the carbon materials not only coat the $Co@Co_3O_4$ nanoparticles, but also form carbon network that connects the $Co@Co_3O_4$ nanoparticles. This conductive carbon network is beneficial to improve the electrochemical performance of the composite. The electrochemical test results show that the $Co@Co_3O_4$@NDC composite exhibits excellent electrochemical performance, delivering the discharge capacities of 790 and 304 $mAh \cdot g^{-1}$ after 1500 cycles at 5 C and 10 C. This excellent electrochemical performance is due to synergistic effects of Co_3O_4, cobalt nanoparticles embedded in carbon which has high conductivity, and nitrogen functional groups.

Keywords: *$Co@Co_3O_4$@Nitrogen doped carbon composite; ionic liquid; lithium ion battery; anode material*

1. Introduction

Lithium-ion batteries (LIBs), as one of the most important energy storage devices, are widely used in mobile phones and hybrid cars [1, 2]. The anode material is one of the most important parts of LIBs. Currently, graphite, the commonly used anode material for commercial LIBs, hinders applications of LIBs due to its low theoretical capacity (372 $mAh \cdot g^{-1}$) and poor cycling at higher current density [3, 4]. Therefore, various studies are being carried out to find a substitute for graphite as anode material of LIBs with high capacity. A variety of binary and ternary oxides, MCo_2O_4 (M=Co, Zn, Cu, Mn, Ni, Fe), nitrides and fluorides, other Ti and Sn based oxides have been studied to replace traditional anode materials for LIBs due to their high specific capacities [4–6]. Among these materials, Co_3O_4 has become the focus of researchers due to its high theoretical specific capacity (896 $mAh \cdot g^{-1}$) and excellent electrochemical reactivity [7]. But Co_3O_4 electrode usually shows low rate capability and rapid capacity fade due to its low electrical conductivity, large volume effect, agglomeration of particles during cycling, and the low Coulombic efficiency [8]. Nanocrystallized structures of Co_3O_4 [9], such as nanoparticle [10], nanorod [11], nanotube [12], and nanofiber [13], is an effective method to improve its electrochemical performance. However, the agglomeration of the nanostructured Co_3O_4 during insertion/extraction of lithium ion still severely affects its electrochemical performance [14]. Recently, integrating nanostructured Co_3O_4 with different types of carbon materials has attracted much attention [15–17]. The carbon material can buffer the volume expansion of Co_3O_4, inhibit the particle agglomeration and shorten the conductive path of lithium ions and

*E-mail: mengyanshuang@163.com

electrons [18]. Nitrogen doping is a commonly used strategy to improve the electrochemical performance of carbon materials [19]. Nitrogen doping can generate many defects on carbon material to create disordered carbon structure, improving the reactivity of carbon materials, thereby enhancing the lithium intercalation properties of carbon materials [20, 21]. Nitrogen groups can also introduce many active sites, increasing the rate performance of materials [22, 23]. Previous research indicated that compounding Sn nanoparticles with N-doped porous carbon could improve the cyclic stability and rate performance [24].

Ionic liquids (ILs) have been studied as carbon and nitrogen sources due to their negligible vapor pressure, high thermal stability and designable structure [25–28]. Negligible vapor pressure makes the carbonization process much easier. Thermal stability makes it possible to polymerize monomers with cross-linking function, making the microstructure and the precursor easier to design, further facilitating controllable preparing of carbon materials. By controlling the proportion of cations and anions in ILs, the structure of carbon materials can be designed and the doping amount of heteroatoms in carbon materials can be adjusted. Therefore, ILs are excellent carbon precursors for LIBs electrode materials.

In this work, we used 1-hexyl-3-methyl imidazolium dilyanamide ([HMIm]N$(CN)_2$) as carbon and nitrogen sources, cobalt acetate as cobalt source to synthesize Co@NDC composite by high temperature pyrolysis. The Co@Co_3O_4@NDC composite was obtained after oxidizing Co@NDC composite at low temperature. The resulting carbon material was wrapped on the surface of Co@Co_3O_4 nanoparticles and formed a network connecting the Co@Co_3O_4 nanoparticles. This special structure not only effectively moderates the volume effect of the Co@Co_3O_4@NDC composite during cycling, but also facilitates the ion transmission, significantly improving the electrochemical performance. When used as anode in LIBs, Co@Co_3O_4@NDC showed specific capacity of 790 mAh·g^{-1} after 1500 cycles at 5 C, revealing the great potential of this novel synthetic method to prepare electrode materials for LIBs.

2. Experimental

2.1. Preparation of Co@Co_3O_4@NDC material

1.02 g cobalt acetate (Co(AC)·$4H_2O$) was dispersed in 1 mL deionized and added to 1.05 g urea ($CO(NH_2)_2$), mixed and ground for 5 min in an agate mortar. Subsequently, 2.03 g [HMIm]N$(CN)_2$ was dropped into the mixture and continuously ground for 30 min. The mixture was then transferred to a ceramic crucible and dried under vacuum at 100 °C for 12 h to remove water and form the precursor. After drying, the precursor was heated to 350 °C for 1 h then heated to 800 °C for 2 h in the argon atmosphere to prepare Co@NDC composite. The heating rate was 5 °C/min during the annealing process. Finally, the Co@NDC composite was oxidized in air for 2 h at 250 °C to obtain Co@Co_3O_4@NDC composite.

2.2. Materials characterization

The crystal structure of the sample was examined by XRD with a Rigaku D/MAX 2500V X-ray diffractometer and Ni filtered CuKα radiation. Data were collected in the 2θ range of 10° to 80° with a scan rate of 2 °/min. Raman spectra were recorded on a Lab RAM HR UV-Vis-NIR (Horiba Jobin Yvon, France) using a CW Ar-ion laser (514.5 nm) as an excitation source. SEM images and the EDS spectra were obtained using a scanning electron microscope (SEM, JEOL-6701F) with the EDS device of Japanese Electronic Optical Company. TEM and HR-TEM images were recorded using a transmission electron micrscope (JEOL JEM-2010F). X-ray photoelectron spectroscopic (XPS) spectra of Co@Co_3O_4@NDC composite were obtained by ESCALAB 250Xi equipped with an aluminum target X-ray source (AlKα, 29.35 eV). The Brunauer-Emmelt-Teller (BET) specific surface and pore size distribution of the materials were calculated using a nitrogen adsorption-desorption measurement at 77 K. The nitrogen and carbon contents were determined by Elementar Analysensysteme GmbH varioEL cube analyzer.

2.3. Electrochemical measurements

Electrochemical performances of Co@Co_3O_4@NDC and Co@NDC composites were measured using half coin cell (CR2032). The working electrode was made by mixing 0.07 g active material, 0.02 g super P and 0.01 g polyvinylidene fluoride (PVDF) in N-methyl pyrrolidone (NMP) until homogeneous slurry was obtained in the agate mortar. Then the slurry was coated onto Cu foil by the smear machine. The solvent was evaporated at 80 °C for 12 h in vacuum. Prepared electrode was used as the working electrode, lithium metal foil as the counter electrode and the Celgard 2400 microporous polypropylene film as a separator. The cell was assembled inside a glove box filled with dry argon. The electrolyte used was a solution of 1 M lithium hexafluorophosphate ($LiPF_6$) in a mixture of ethylene carbonate (EC) and diethyl carbonate (DEC) with a volume ratio of 1:1. Land CT2001A was used for the analysis of cell performance by constant charge-discharge testing, cyclic voltammetry (CV) and electrochemical impedance spectra (EIS).

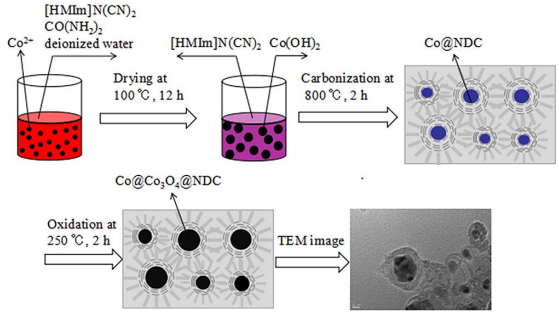

Fig. 1. Schematic of the synthesis process for Co@Co_3O_4@NDC composite.

3. Results and discussion

The schematic of the synthesis process for Co@Co_3O_4@NDC composite is shown in Fig. 1. The mixture is dried at 100 °C to form the $Co(OH)_2$ precursor. Next, the mixture is firstly stabilized at 800 °C in the argon atmosphere to obtain Co@NDC composite and then, a part of cobalt metal in the Co@NDC composite is oxidized to form the Co@Co_3O_4@NDC composite at 250 °C in air. There is a little loss of carbon material during the oxidizing process. In the process of high temperature carbonization, not only onion carbon is catalyzed due to cobalt coats on the surface of Co@Co_3O_4 nanoparticles, but also other amorphous carbon forms a conductive network to connect Co@Co_3O_4@NDC particles.

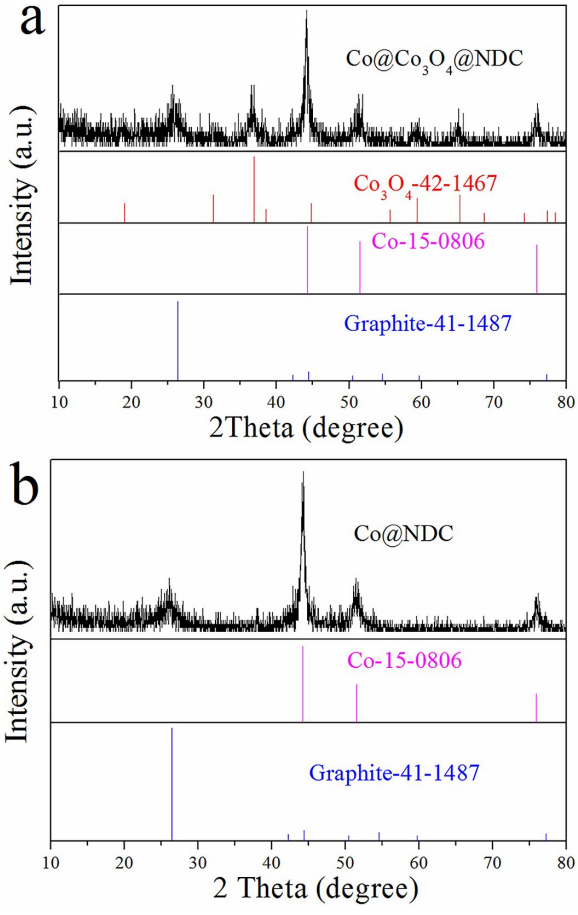

Fig. 2. XRD patterns of Co@Co_3O_4@NDC (a) and Co@NDC (b).

Fig. 2 shows the XRD patterns of Co@Co_3O_4@NDC and Co@NDC, respectively. The Co@Co_3O_4@NDC composite exhibits the characteristic peaks of Co_3O_4, Co, and carbon. The diffraction peak at 26° corresponds to the (0 0 2) crystal plane of graphitic carbon (Fig. 2a) [29]. The additional peaks are assigned to the cubic phase of spinel-structured Co_3O_4

(Co_3O_4-42-1467) and the face-centered-cubic cobalt (Co-15-0806), indicating that part of the cobalt metal has been oxidized to Co_3O_4 [30, 31]. XRD pattern of Co@NDC (Fig. 2b) shows the sharp peaks of carbon and cobalt without other phase, indicating a high crystallinity and purity of the Co@NDC [32]. Metal Co is reduced from Co^{2+} by the carbon generated by the pyrolysis of ILs in the inert atmosphere [33].

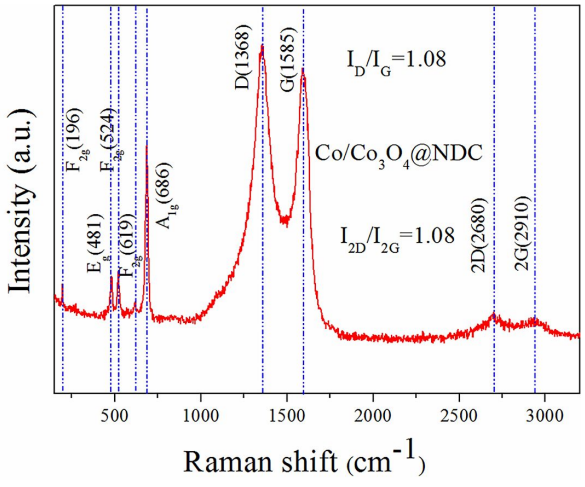

Fig. 3. Raman spectrum of Co@Co_3O_4@NDC composite.

Fig. 3 shows the Raman spectrum of Co@Co_3O_4@NDC composite. The characteristic peaks at ~1368 cm^{-1} and ~1585 cm^{-1} are associated with the D and G band of sp^3-hybridized and sp^2-hybridized carbon vibrations, respectively [34, 35]. The intensity ratio (I_D/I_G) is 1.08, indicating that the graphitization degree of Co@Co_3O_4@NDC composite is relatively high, which is very favorable for its high electrochemical performance [36, 37]. Other peaks at 189 cm^{-1}, 458 cm^{-1}, 510 cm^{-1}, 601 cm^{-1} and 670 cm^{-1} can be assigned to the F_{2g}, E_g, $F^1{}_{2g}$, $F^2{}_{2g}$ and A_{1g} modes of Co_3O_4, indicating the presence of Co_3O_4 nanoparticles in the Co@Co_3O_4@NDC composite [35]. The intensity ratio of 2D peak (2680 cm^{-1}) to 2G peak (2910 cm^{-1}) is very sensitive to dopants and defects [38–40]. The I_{2D}/I_{2G} ratio of the composite is nearly 1.08, indicating that the nitrogen atoms are successfully doped into the carbon structure.

The specific surface area and pore size distribution of Co@Co_3O_4@NDC composite were analyzed by nitrogen adsorption/desorption measurement in Fig. 4a. The BET specific surface area of Co@Co_3O_4@NDC composites is calculated to be 81.6 $m^2 \cdot g^{-1}$, and the average pore size is 3.81 nm. The high specific surface area can be largely attributed to the onion carbon structure formed by cobalt catalysis, which is beneficial to improve the electrochemical performance of Co@Co_3O_4@NDC composite.

The XPS spectra of Co@Co_3O_4@NDC composite are shown in Fig. 4b, Fig. 4c, Fig. 4d, Fig. 4e and Fig. 4f. In Fig. 4b, the peaks corresponding to C 1s, N 1s, O 1s and Co $2p_{3/2}$ indicate that the composite is composed of C, N, O and Co. In the Co $2p_{3/2}$ spectrum (Fig. 4c), the peaks at 780.6 eV, 779.9 eV, and 780.9 eV are attributed to Co, Co^{3+} and Co^{2+}, indicating the existence of Co_3O_4 in the composite [33, 41]. The O 1s spectrum (Fig. 4d) splits into two distinct peaks at 530.2 eV and 531.8 eV, which can be assigned to Co–O and C–O bonds, respectively, further confirming the presence of Co_3O_4 [42]. As shown in Fig. 4e, the C 1s spectrum splits into three peaks at 284.7 eV, 285.6 eV, and 285.7 eV, respectively. The peak at 284.7 eV corresponds to the C=C bond [43]. The peak at 285.6 eV is due to the C–O bond, yielding a C–O–Co bond that binds the carbon material to Co_3O_4 [44, 45]. The peak at 285.7 eV is designated to the C–N bond [46]. In Fig. 4f, N 1s spectrum indicates the presence of pyridinic N (398.7 eV), pyrrolic N (399.6 eV), and graphitic N (401.3 eV) [47]. Previous researches have reported that the N-doped carbon can improve conductivity and electrochemical activity of material [19]. Pyrrolic N can provide two electrons to the π system to produce many defects, forming electrochemical active sites, thereby increasing the lithium storage capacity of Co@Co_3O_4@NDC composite. Graphitic N can enhance electron conductivity, improving the electrochemical performance of Co@Co_3O_4@NDC composite [48]. The results are in accordance with the Raman results.

The SEM image of Co@Co_3O_4@NDC composite is shown in Fig. 5a. The Co@Co_3O_4@NDC composite exists in the form of spherical

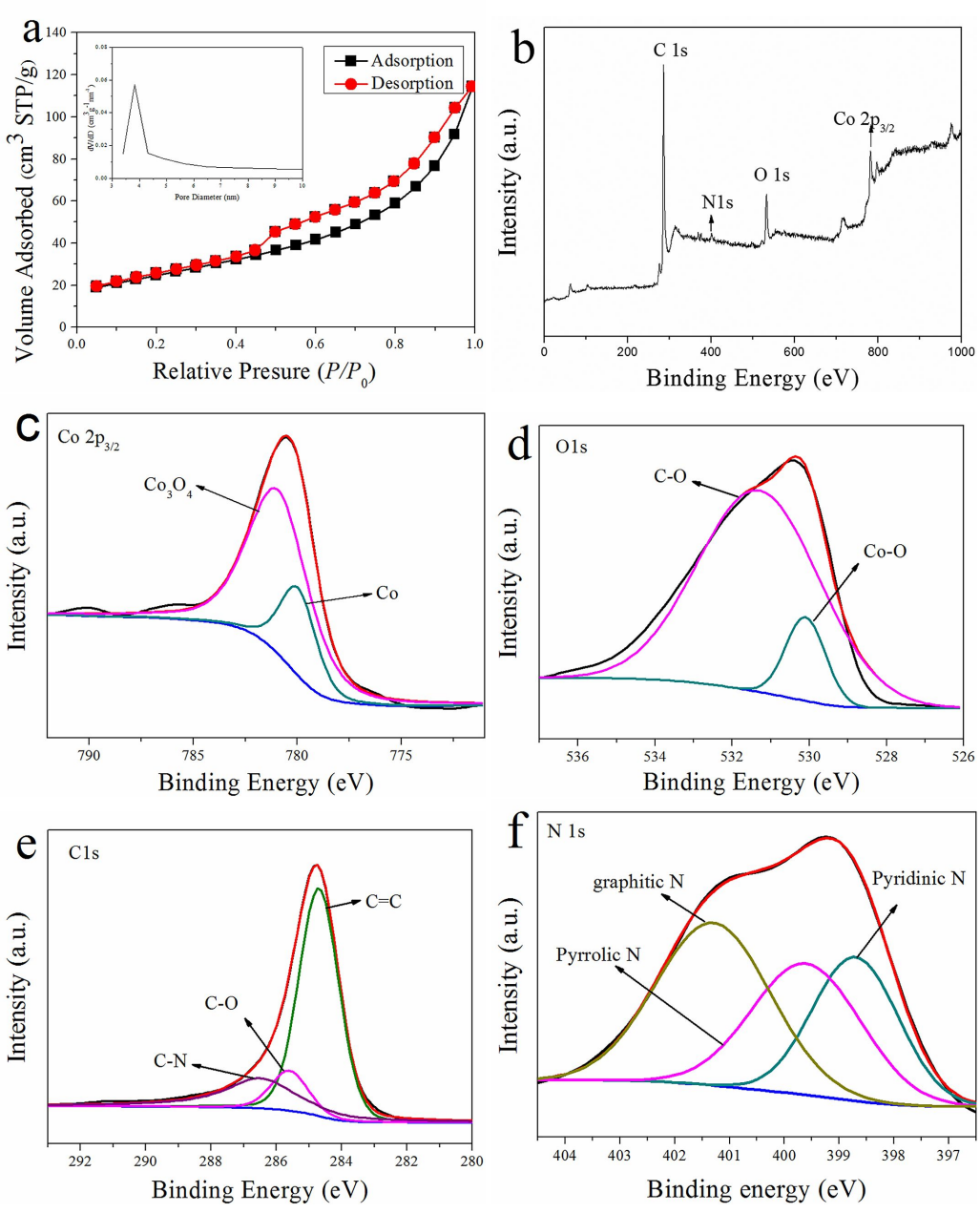

Fig. 4. N_2 adsorption/desorption isotherms and corresponding pore size distribution curves (the inset) of (a) Co@Co_3O_4@NDC composite; XPS survey spectrum (b) and high-resolution XPS spectra of Co $2p_{3/2}$ (c), O 1s (d), C 1s (e), and N 1s (f) of Co@Co_3O_4@NDC composite.

nanoparticles. The carbon materials with onion carbon structure and a conductive network can effectively prevent the agglomeration of Co@Co_3O_4 nanoparticles and inhibit the volume effect of Co_3O_4. The elemental mappings show that the Co@Co_3O_4@NDC composite has Co, C, O and N elements (Fig. 5b, Fig. 5c, Fig. 5d, Fig. 5e and Fig. 5f). The Co, C, O and N elements are uniformly distributed in the Co@Co_3O_4@NDC composite with the elements mass contents of about 39.15 %, 5.26 %, 54.21 % and 1.37 %, respectively. Thus it is concluded that Co_3O_4 and

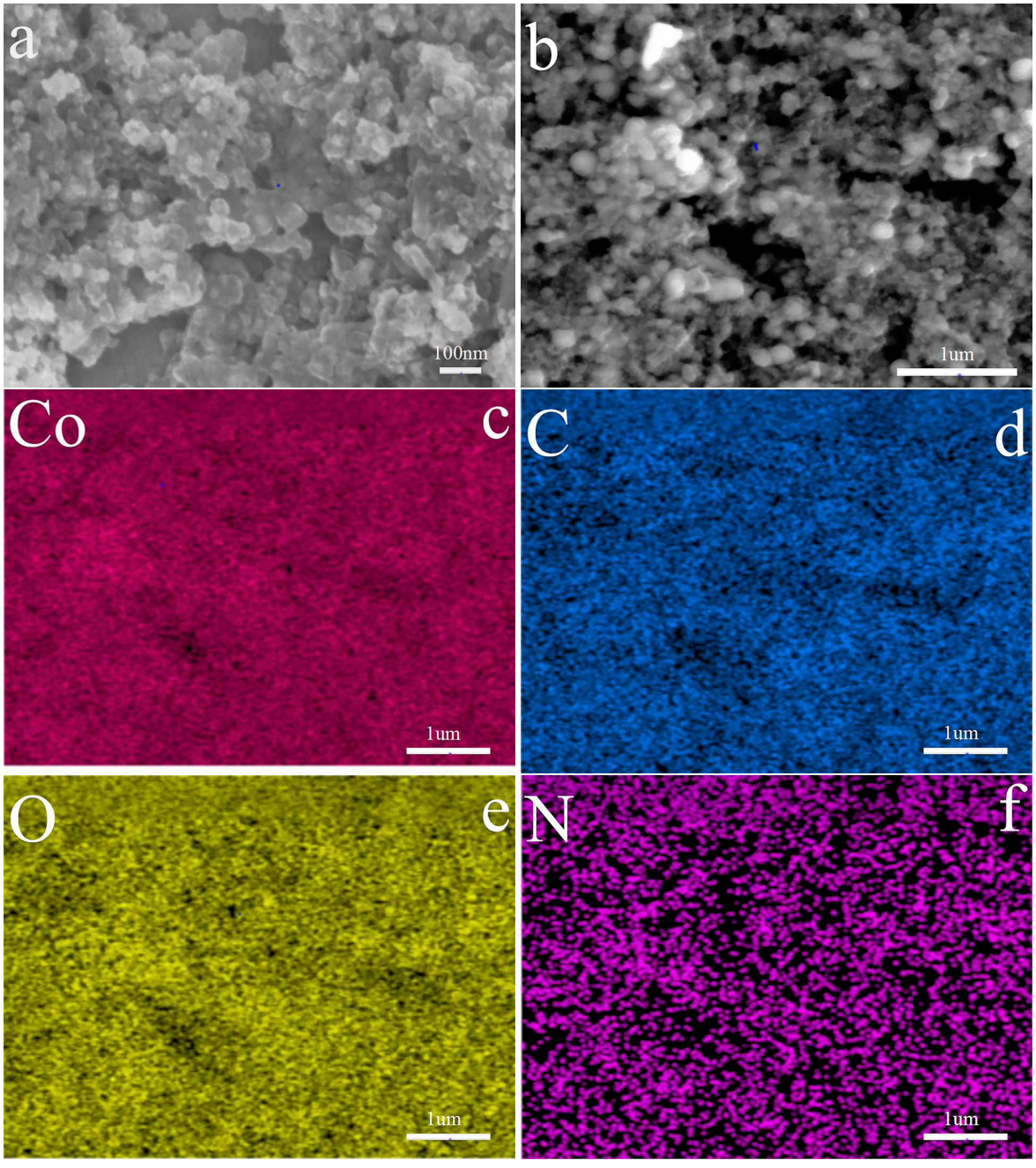

Fig. 5. SEM images (a) and EDS elemental mappings (b), (c), (d), (e), (f) of Co@Co_3O_4@NDC composite.

Co mass contents are 19.8 % and 24.62 %. The nitrogen and carbon contents in Co@Co_3O_4@NDC sample determined by elemental analysis are 1.81 % and 53.27 %.

TEM images of Co@NDC and Co@Co_3O_4@NDC composite are shown in Fig. 6. Compared with the Co@NDC composite (Fig. 6a), the Co@Co_3O_4@NDC composite (Fig. 6b) has a low carbon content due to the partial conversion of carbon to CO_2 during low temperature oxidation. In Fig. 6b, a less intensive effect of Co@Co_3O_4 nanoparticles is observed, possibly due to the contact between Co@Co_3O_4 nanoparticles, when carbon materials are consumed during oxidation process. In Fig. 6c, the Co@Co_3O_4 particles with a particle size of about 30 nm are coated with

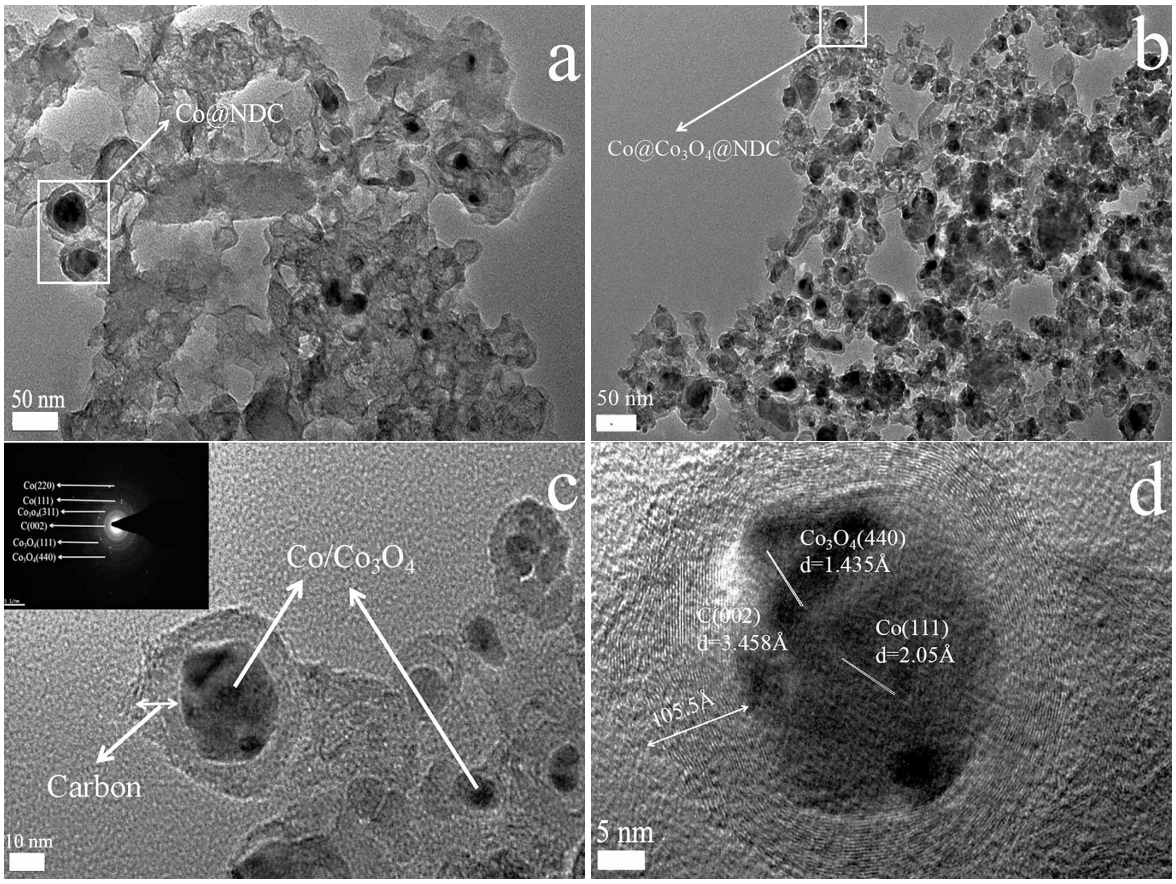

Fig. 6. TEM image of Co@NDC composite (a); TEM image of Co@Co_3O_4@NDC (b), SAED pattern (c) and HR-TEM image (d) of Co@Co_3O_4@NDC composite.

carbon. Carbon not only forms onion carbon structure wrapped on the Co@Co_3O_4 particles, but also forms a conductive network structure to promote the transport of electrons and lithium ions. The SAED pattern shows the diffraction points and diffraction rings of Co_3O_4-42-1467 and Co-15-0806, which is consistent with the XRD results, further confirming the presence of Co and Co_3O_4 [49, 50]. The d-spacing value estimated from the rings matches well with the d-spacing value of graphite-41-1487. The HR-TEM image in Fig. 6d clearly shows the lattice fringes, corresponding to the C (0 0 2), Co_3O_4 (4 4 0), and Co (1 1 1) planes [33]. The carbon materials show onion-like morphology with the thickness of about 10.55 nm. The Co@Co_3O_4 nanoparticles are anchored with the onion-like carbon. This is because [(BMIm)N$(CN)_2$] has good wettability and helps it penetrate into Co@Co_3O_4 particles during carbonization [51, 52].

The electrochemical performance of the Co@Co_3O_4@NDC composite is shown in Fig. 7a. The specific capacities of the Co@Co_3O_4@NDC are 790 mAh·g^{-1} and 304 mAh·g^{-1} after 1500 cycles at 5 C and 10 C, respectively, demonstrating its excellent rate performance. Its specific capacity increases gradually during cycling, which can be attributed to the fact that the solid electrolyte interphase (SEI) film can be electrocatalytically decomposed by metal Co and gradually form a stable SEI film during discharge/charge [53, 54]. In Fig. 7b, the initial discharge/charge capacities of Co@Co_3O_4@NDC and Co@NDC composite are 1308/834 mAh·g^{-1} and 1031/534 mAh·g^{-1} at 0.5 C, respectively. Co@Co3O4@NDC composite exhibited 63.75 % Coulombic efficiency at the first

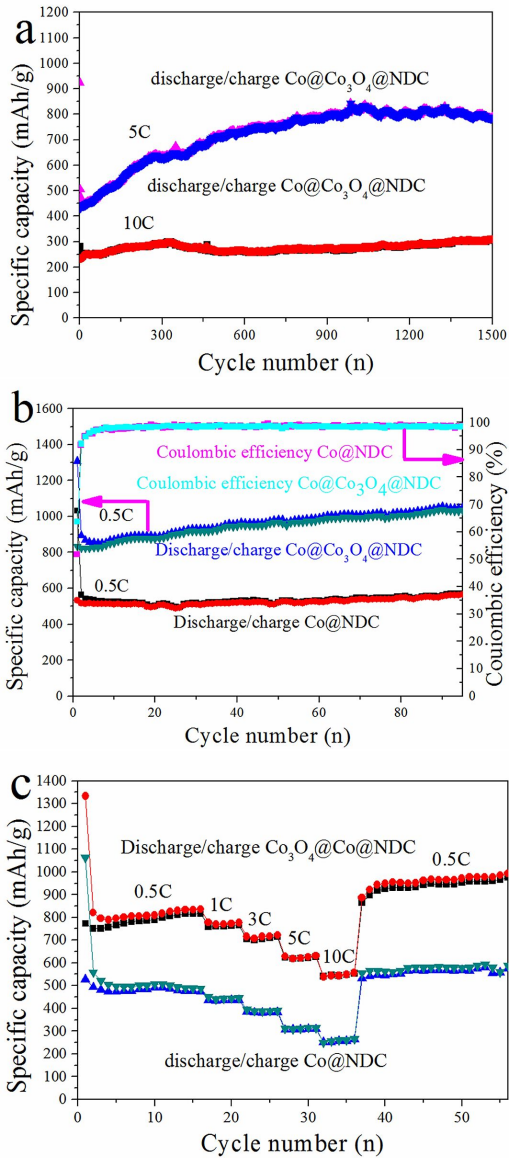

Fig. 7. (a) Cycling performances of the Co@Co_3O_4@NDC composite at 5 C and 10 C; (b) cycling performances and Coulombic efficiency of the Co@NDC and Co@Co_3O_4@NDC composite at 0.5 C; (c) rate capability of Co@Co_3O_4@NDC composite at various current densities ranging from 0.5 C to 10 C.

cycle, which was higher than that of Co@NDC composite (51.74 %). Irreversible capacity loss is mainly due to incomplete conversion reaction, irreversible lithium loss caused by formation of SEI film in the first cycle [55, 56]. This results show that Co@NDC composite is more likely to form a thick SEI film [49]. The discharge specific capacities of Co@Co_3O_4@NDC and Co@NDC composite are 1049 and 571 mAh·g^{-1} after 95 cycles at 0.5 C, respectively. Co@Co_3O_4@NDC composite has higher capacity than Co@NDC composite, and Co@Co_3O_4@NDC composite capacity growth is more obvious. Fig. 7c shows the rate capabilities of Co@Co_3O_4@NDC and Co@NDC composite at a current density from 0.5 C to 10 C. Co@Co_3O_4@NDC shows better rate capability than Co@NDC. The specific capacity of Co@Co_3O_4@NDC composite reaches 409 mAh·g^{-1} even at 10 C, while Co@NDC composite is only 252 mAh·g^{-1}. Excellent comprehensive electrochemical performance of Co@Co_3O_4@NDC composite is due to the synergistic effects of high capacity of Co_3O_4, superior conductivity of onion carbon and cobalt metal, and N functional groups, which can shorten the ion transport pathways and inhibit the volume effect during cycling.

The charge-discharge curves of Co@Co_3O_4@NDC and Co@NDC composite at 0.5 C during the first-three cycles are shown in Fig. 8a and Fig. 8b, respectively. Obviously, Co@Co_3O_4@NDC composite has two more longer platforms at ~0.86 V and 2.01 V than Co@NDC composite during the first discharge/charge, which stem from Co_3O_4 in the Co@Co_3O_4@NDC composite [57]. In Fig. 8a, the charge-discharge curves of characteristic Co_3O_4 are not obvious because the carbon content is higher than Co_3O_4 content. There are no significant changes in the charge-discharge curves between the 2nd and 3rd cycle, indicating that the prepared Co@Co_3O_4@NDC composite has good cycling performance [58]. Fig. 8c and Fig. 8d are the CV curves of Co@Co_3O_4@NDC and Co@NDC composite in the first-three cycles, respectively. In Fig. 8c, in the first cathodic scan, an irreversible peak at 1.01 V has aroused by the formation of an intermediate product $Li_xCo_3O_4$ (Co_3O_4 + xLi^+ ↔ $Li_xCo_3O_4$) [59]. The strong peak at 0.86 V is attributed to the electrochemical reduction reaction of Co_3O_4 to Co^0 metal and amorphous Li_2O (Co_3O_4 + 8Li^+ + 8e^- ↔ 4Li_2O + 3Co^0) [60]. The peaks at 1.2 V and 2.01 V are due

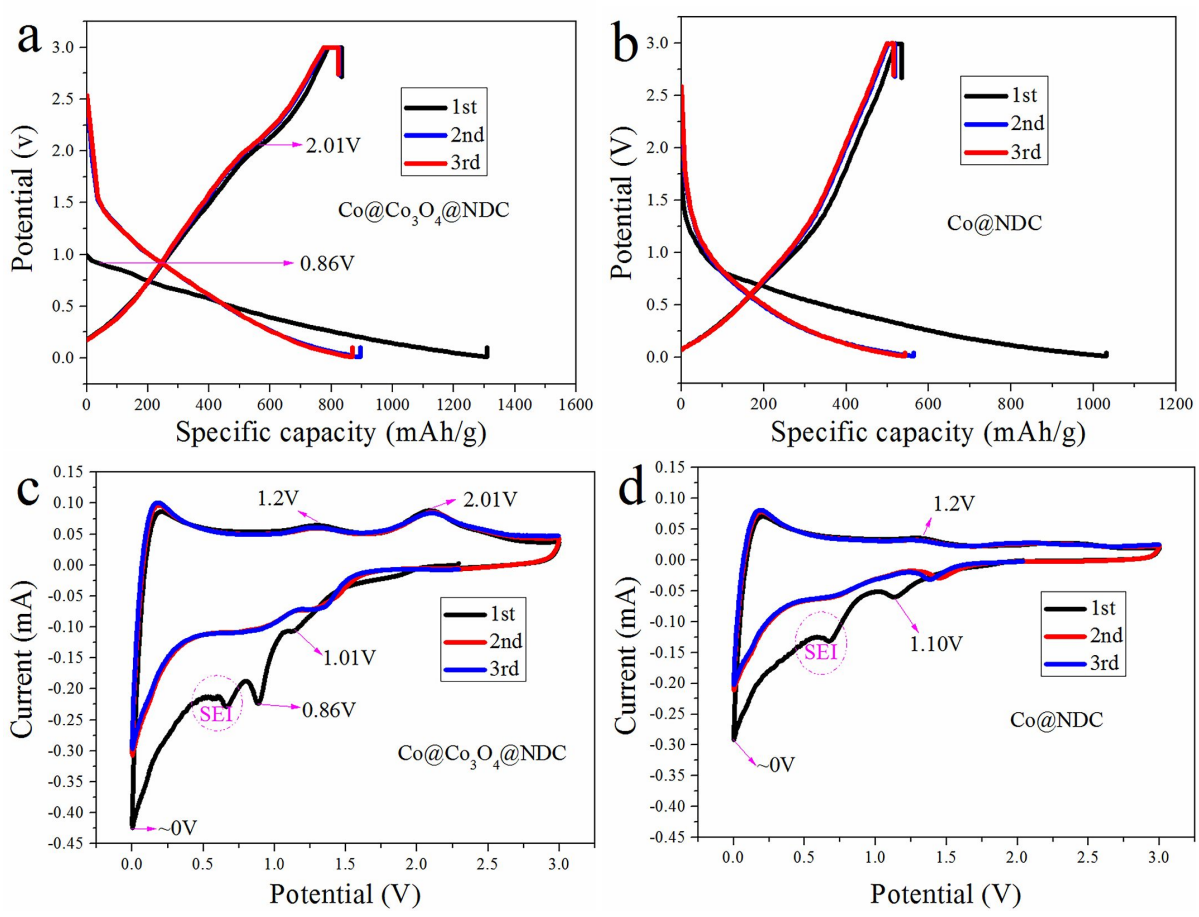

Fig. 8. First-three-cycle charge-discharge profiles of (a) Co@Co_3O_4@NDC and (b) Co@NDC composite at 0.5 C; first-three cycles CV curves of (c) Co@Co_3O_4@NDC and (d) Co@NDC composite at a scanning rate of 0.2 mV·s^{-1} in the potential range of 0 V to ~3.0 V.

to the decomposition of Li_2O and the re-oxidation of cobalt metal to Co_3O_4 [61]. For comparison, the CV curves of Co@NDC composite are shown in Fig. 8d. The peak at 1.1 V corresponds to the Li_x-Co alloy formed between Co and Li species [62]. The oxidation peak at 1.2 V is attributed to the Li^+ extraction process [58]. For both samples, there is a sharp voltage drop below ~0.6 V, which is related to the decomposition of electrolyte and SEI film formation [63]. This is also the main reason for the lower initial Coulombic efficiency for the first cycle. The sharp peak at 0 V is associated with the insertion of Li^+ into the carbon layer [49, 57], indicating capacity contribution of the carbon materials. From the third cycle, the redox peak almost completely coincides with the second cycle, indicating that the Co@Co_3O_4@NDC composite has excellent reversibility and integrity [64].

Nyquist plot is composed of the electrolyte resistance (Re) and the surface film resistance (Rs) at high frequency, the charge transfer resistance (R1) at intermediate frequency, and sloped line at low frequency indexed with the Warburg resistance (W1) [65, 66]. To further study the reason for that Co@Co_3O_4@NDC composite has excellent electrochemical performance, the Nyquist plot after 10 cycles at 0.005 V in the frequency range of 0.01 Hz to 10^5 Hz has been measured and shown in Fig. 9a. In Fig. 9a, the symbols show the experimental data, whereas the continuous lines represent the fitting curves. Typical parameters are summarized in the inset table.

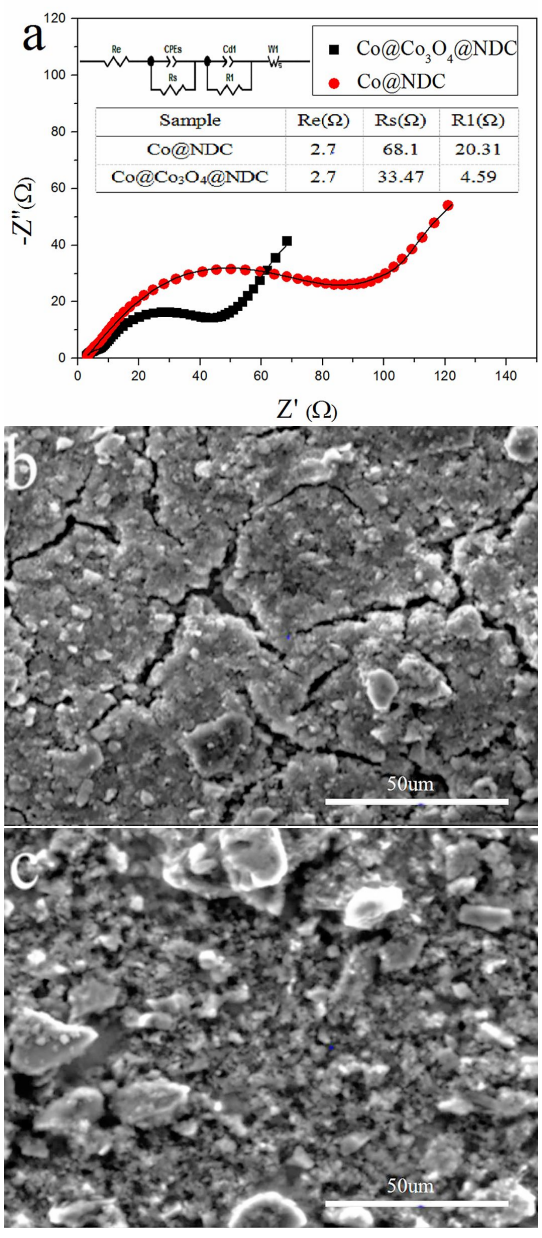

Fig. 9. (a) Nyquist plots of Co@NDC and $Co@Co_3O_4@NDC$ composite after 10 cycles, SEM images of Co@NDC composite (b) and $Co@Co_3O_4@NDC$ composite (c) after 10 cycles. Inset: the equivalent electric circuit used to fit the EIS plots and the fitted Re, Rsf and Rct values.

The SEI film resistances of $Co@Co_3O_4@NDC$ and Co@NDC are 33.47 Ω and 68.1 Ω, and the charge transfer resistances are 4.59 Ω and 20.31 Ω, respectively, suggesting that $Co@Co_3O_4@NDC$ composite has much better charge transfer ability. Therefore, the $Co@Co_3O_4@NDC$ composite has better electrochemical performance [65]. SEM images of both samples after 10 cycles are shown in Fig. 9b and Fig. 9c. The Co@NDC composite does not have a clear morphology such as $Co@Co_3O_4@NDC$ composite, indicating the SEI film of Co@NDC composite is obviously thicker than that of $Co@Co_3O_4@NDC$ composite [49], and the SEI film resistance of Co@NDC composite is higher than that of $Co@Co_3O_4@NDC$. The thick SEI film with low conductivity is not conducive to electrochemical performance, which leads to an increase in charge transfer resistance.

4. Conclusions

The $Co@Co_3O_4@NDC$ composite has been prepared by using $[HMIm]N(CN)_2$ as carbon and nitrogen source. This special structure of the composite can moderate the volume effect of Co_3O_4 during cycling and shorten the lithium ions and electrons transport pathways. Therefore, the $Co@Co_3O_4@NDC$ as anode exhibits excellent electrochemical performance due to synergistic effects of the high capacity of Co_3O_4 nanoparticles, cobalt nanoparticles embedded in carbon having high conductivity, and the active sites of N-functional groups. The $Co@Co_3O_4@NDC$ composite delivered the discharge capacities of 790 and 304 $mAh \cdot g^{-1}$ after 1500 cycles at 5 C and 10 C, respectively.

Acknowledgements

The project was supported by the National Natural Science Foundation of China (Grant No. 51364024 and 51404124), and the Foundation for Innovation Groups of Basic Research in Gansu Province (No. 1606RJIA322).

References

[1] LIANG S., ZHU X., LIAN P., YANG W., WANG H., *J. Solid State Chem.*, 184 (6) (2011), 1400.

[2] CHERIAN C.T., SUNDARAMURTHY J., REDDY M.V., SURESH K.P., MANI K., PLISZKA D., SOW C.H., RAMAKRISHNA S., CHOWDARI B.V., *ACS App. Mater. Interface.*, 5 (20) (2013), 9957.

[3] BAI L.-Z., ZHAO D.-L., ZHANG T.-M., XIE W.-G., ZHANG J.-M., SHEN Z.-M., *Electrochim. Acta*, 107 (2013), 555.

[4] REDDY M.V., CAI Y., FAN J., LOH K.P., CHOWDARI B.V.R., *RSC Adv.*, 2 (25) (2012), 9619.

[5] REDDY M.V., ZHANG B., LOH K.P., CHOWDARI B.V.R., *Crystengcomm.*, 15 (18) (2013), 3568.

[6] REDDY M.V., KENRICK K.Y.H., TANG Y.W., CHONG G.Y., LEONG G.H., CHOWDARI B.V.R., *J. Electrochem. Soc.*, 158 (12) (2011), A1423.

[7] YANG X., FAN K., ZHU Y., SHEN J., JIANG X., ZHAO P., LUAN S., LI C., *Appl. Mater. Interface.*, 5 (3) (2013), 997.

[8] WU H., DU N., WANG J., ZHANG H., YANG D., *J. Power Sources*, 246 (2014), 198.

[9] WU H.B., CHEN J.S., HNG H.H., LOU X.W., *Nanoscale*, 4 (8) (2012), 2526.

[10] HUANG Y., CHEN C., AN C., XU C., XU Y., WANG Y., JIAO L., YUAN H., *Electrochim. Acta*, 145 (2014), 34.

[11] ZHANG H., WU J., ZHAI C., MA X., DU N., TU J., YANG D., *Nanotechnolog.*, 19 (3) (2008), 035711.

[12] LOU X.W., DENG D., LEE J.Y., FENG J., ARCHER L.A., *Adv. Mater.*, 20 (2) (2008), 258.

[13] YANG X., FAN K., ZHU Y., SHEN J., JIANG X., ZHAO P., LUAN S., LI C., *ACS Appl. Mater. Interface.*, 5 (3) (2013), 997.

[14] HUANG G., XU S., LU S., LI L., SUN H., *ACS Appl. Mater. Interface.*, 6 (10) (2014), 7236.

[15] CHEN J., XIA X.-H., TU J.-P., XIONG Q.-Q., YU Y.-X., WANG X.-L., GU C.-D., *J. Mater. Chem.*, 22 (30) (2012), 15056.

[16] XU J., WU J., LUO L., CHEN X., QIN H., DRAVID V., MI S., JIA C., *J. Power Sources*, 274 (2015), 816.

[17] WANG F., LIANG L., SHI L., LIU M., SUN J., *J. Alloy. Compd.*, 633 (2015), 65.

[18] ABOUALI S., AKBARI GARAKANI M., ZHANG B., LUO H., XU Z.-L., HUANG J.-Q., HUANG J., KIM J.-K., *J. Mater. Chem. A*, 2 (40) (2014), 16939.

[19] WANG X., LI X., ZHANG L., YOON Y., WEBER P.K., WANG H., GUO J., DAI H., *Science*, 324 (5928) (2009), 768.

[20] LIU Y., LIU L., KONG L., KANG L., RAN F., *Electrochim. Acta*, 211 (2016), 469.

[21] LIU Q., PU Z., TANG C., ASIRI A.M., QUSTI A.H., AL-YOUBI A.O., SUN X., *Electrochem. Commun.*, 36 (6) (2013), 57.

[22] ZHOU Z., GAO X., YAN J., SONG D., MORINAGA M., *Carbon*, 42 (12 – 13) (2004), 2677.

[23] MA C., SHAO X., CAO D., *J. Mater. Chem.*, 22 (18) (2012), 8911.

[24] ZHU Z., WANG S., DU J., JIN Q., ZHANG T., CHENG F., CHEN J., *Nano Lett.*, 14 (1) (2014), 153.

[25] MENG Y., XIA J., ZHU FL., ZHANG Y., *Int. J. Electrochem. Sci.*, 11 (12) (2016), 9881.

[26] WANG X., DAI S., *Angewandte Chem. Int. Ed.*, 49 (37) (2010), 6664.

[27] FULVIO P.F., LEE J.S., MAYES R.T., WANG X., MAHURIN S.M., DAI S., *Phys. Chem. Chem. Phys. Pccp.*, 13 (30) (2011), 13486.

[28] SUN S., LANG J., WANG R., KONG L., LI X., YAN X., *J. Mater. Chem. A*, 2 (35) (2014), 14550.

[29] ZHAO S., LIU W., LIU S., ZHANG Y., WANG H., CHEN S., *Electrochim. Acta*, 231 (2017), 511.

[30] JIANG Y., YAN X., XIAO W., TIAN M., GAO L., QU D., TANG H., *J. Alloy. Compd.*, 710 (2017), 114.

[31] WU Z.S., REN W., WEN L., GAO L., ZHAO J., CHEN Z., ZHOU G., LI F., CHENG H.M., *ACS Nano.*, 4 (6) (2010), 3187.

[32] ZHANG P., GUO Z.P., HUANG Y., JIA D., LIU H.K., *J. Power Sources*, 196 (16) (2011), 6987.

[33] ZHOU K., LAI L., ZHEN Y., HONG Z., GUO J., HUANG Z., *Chem. Eng. J.*, 316 (2017), 137.

[34] LI B., CAO H., SHAO J., LI G., QU M., YIN G., *Inorg. Chem.*, 50 (5) (2011), 1628.

[35] LI M., XU S., ZHU Y., XU Y., YANG P., WANG L., CHU P.K., *Mater. Lett.*, 132 (2014), 405.

[36] ZHOU M., PU F., WANG Z., GUAN S., *Carbon*, 68 (3) (2014), 185.

[37] FERRARI A.C., MEYER J.C., SCARDACI V., CASIRAGHI C., LAZZERI M., MSURI F., PISCANEC S., JIANG D., NOVOSELOV K.S., ROTH S., *Phys. Rev. Lett.*, 97 (18) (2006), 187401.

[38] JIN Z., YAO J., KITTRELL C., TOUR J.M., *ACS Nano.*, 5 (5) (2011), 4112.

[39] TANG X., FENG Q., HUANG J., LIU K., LUO X., PENG Q., *J. Colloid Interf. Sci.*, 510 (2018), 368.

[40] JIE W., HUI Y.Y., ZHANG Y., SHU P.L., HAO J., *Appl. Phys. Lett.*, 102 (22) (2013), 223112.

[41] HUANG W., ZUO Z., HAN P., LI Z., ZHAO T., *J. El. Spectrosc. Rel. Phenom.*, 173 (2) (2009), 88.

[42] REDDY M.V., XU Y., RAJARAJAN V., OUYANG T., CHOWDARI B.V.R., *ACS Sustain. Chem. Eng.*, 3 (12) (2015), 3035.

[43] LI W., ZHENG Y., WANG X., CHEN S., XU F., LI Z., WU J., SUN L., ZHUANG L., HOU H., *ACS Appl. Mater. Interf.*, 6 (10) (2014), 7117.

[44] LI D., SHI D., CHEN Z., LIU H., JIA D., GUO Z., *RSC Advs.*, 3 (15) (2013), 5003.

[45] MAO Y., DUAN H., XU B., ZHANG L., HU Y., ZHAO C., WANG Z., CHEN L., YANG Y., *Energ. Environ. Sci.*, 5 (7) (2012), 7950.

[46] WONG W.Y., DAUD W.R.W., MOHAMAD A.B., KADHUM A.A.H., LOH K.S., MAJLAN E.H., *Int. J. Hydrogen Energ.*, 38 (22) (2013), 9421.

[47] LI X., ZHU X.B., ZHU Y., YUAN Z., SI L.L., QIAN Y., *Carbon*, 69 (2) (2014), 515.

[48] CHEN T., PAN L., LOH T.A., CHUA D.H., YAO Y., CHEN Q., LI D., QIN W., SUN Z., *Dalton T.*, 43 (40) (2014), 14931.

[49] YAN Z., HU Q., YAN G., LI H., SHIH K., YANG Z., LI X., WANG Z., WANG J., *Chem. Eng. J.*, 321 (2017), 495.

[50] RAMESH S., HALDORAI Y., SIVASAMY A., KIM H.S., *Mater. Lett.*, 206 (2017), 39.

[51] YIN F., YINGYING L., RENCHAO C., HAOYU W., XUEHUA Z., DONG G., GENGFENG Z., DONGYUAN Z., *J. Am. Chem. Soc.*, 135 (4) (2013), 1524.

[52] MENG Y., HAN W., ZHANG Z., ZHU F., ZHANG Y., WANG D., *J. Nanosci. Nanotechnol*., 17 (3) (2017), 2000.
[53] SU L., ZHONG Y., ZHOU Z., *J. Mater. Chem. A*, 1 (47) (2013), 15158.
[54] REN G., HOQUE M.N.F., LIU J., WARZYWODA J., FAN Z., *Nano Energ*., 21 (2016), 162.
[55] YAO W., YANG J., WANG J., NULI Y., *J. Electrochem. Soc*., 155 (12) (2008), A903.
[56] NAM K.T., KIM D.W., YOO P.J., CHIANG C.Y., MEETHONG N., HAMMOND P.T., CHIANG Y.M., BELCHER A.M., *Science*, 312 (5775) (2006), 885.
[57] MARZUKI N.S., TAIB N.U., HASSEN M.F., IDRIS N.H., *Electrochim. Acta*, 182 (2015), 452.
[58] SUN X., SI W., LIU X., DENG J., XI L., LIU L., YAN C., SCHNIDT O.G., *Nano Energ*., 9 (2014), 168.
[59] REDDY M.V., BEICHEN Z., NICHOLETTE L.J.E., KAIMENG Z., CHOWDARI B.V.R., *Electrochem. Solid-State Lett*., 14 (5) (2011), A79.
[60] ZHAN L., CHEN H., FANG J., WANG S., DING L.-X., LI Z., ASHMAN P.J., WANG H., *Electrochim. Acta*, 209 (2016), 192.
[61] KIM G.-P., NAM I., KIM N.D., PARK J., PARK S., YI J., *Electrochem. Commun*., 2 (2012), 93.
[62] LI G.-C., HAO W., *J. Alloy. Compd*., 716 (2017), 156.
[63] WANG J., ZHANG Q., LI X., XU D., WANG Z., GUO H., ZHANG K., *Nano Energ*., 6 (3) (2014), 19.
[64] XING X., LIU R., LIU S., XIAO S., XU Y., WANG C., WU D., *Electrochim. Acta*, 194 (2016), 310.
[65] MAI Y.J., TU J.P., GU C.D., WANG X.L., *J. Power Sources*, 209 (2012), 1.
[66] MARKOVSKY B., RODKIN A., COHEN Y.S., PALCHIK O., LEVI E., AURBACH D., KIM H.J., SCHMIDT M., *J. Power Sources*, 119 – 121 (6) (2003), 504.

Received 2018-07-25
Accepted 2019-04-23